

Free energy of a long semiflexible polymer confined in a spherical cavity

Cite this: *Soft Matter*, 2014, 10, 4674Jie Gao,^a Ping Tang,^{*a} Yuliang Yang^a and Jeff Z. Y. Chen^{*b}Received 20th March 2014
Accepted 16th April 2014

DOI: 10.1039/c4sm00605d

www.rsc.org/softmatter

The free energy and conformational properties of a wormlike chain confined inside a spherical surface are investigated. We show that in the weak-confinement limit, the wormlike chain model exactly reproduces the confinement properties of a Gaussian chain; in such a case the confinement entropy dominates the free energy; in the strong-confinement limit, the free energy is dominated by the bending energy of the chain, which is forced to wrap around the confining surface. We also present a numerical solution within the crossover region between the two limits, solving the differential equation that the probability distribution function satisfies.

1 Introduction

The wormlike chain model is suitable for describing a semiflexible polymer, in which two length scales are important: the total chain contour length L and its persistence length λ .^{1–3} The latter is the orientation–orientation correlation length, below which the polymer appears rigid, along the polymer chain. A wormlike-chain confinement problem typically introduces a third length scale, R . For a long polymer chain ($L/\lambda \gg 1$), the free energy and conformational properties of the confined wormlike chain are controlled by the competition between the two length scales, λ and R .

The study of a wormlike chain confined inside a tube or within a slit has seen significant progress in recent years based on models with and without the excluded volume effects between polymer segments.^{4–25} In contrast, despite recent efforts,^{12,26–29} the problem of a wormlike chain confined inside a spherical cavity of radius R is less understood. The current paper focuses on presenting a complete physical picture resulted from the standard wormlike-chain model for such a case. We will show that two limits exist: in the strong-confinement limit the physical properties are bending-energy dominating and in the weak-confinement limit, entropy dominating. In comparison, the physical properties of a wormlike chain strongly confined in a slit or tube are dominated by the deflection picture presented originally by Odijk,^{4,30} where the entropy still plays a role but in a different manner.

For the purpose of examining the crossover of the wormlike-chain free energy to the Gaussian-chain free energy, we relate λ to the effective Kuhn length a by $a = 2\lambda$, which is a relation

established later in Section 3.2. Using a as the basic length scale, in this work, we show that in the asymptotic limit of strong confinement, $R \ll a \ll L$, the free energy of the confined wormlike chain can be written in a power-law form

$$\beta F = \frac{L}{a} \left[A \left(\frac{a}{R} \right)^2 + \dots \right]. \quad (1)$$

Through an analysis of the monomer distribution of the system, we can also show that the average monomer-to-center distance, $\langle r \rangle$, follows the asymptotic behavior in this limit,

$$\frac{\langle r \rangle}{R} = 1 - \left[\alpha \left(\frac{R}{a} \right) + \dots \right], \quad (2)$$

where α is a numerical coefficient. Another interesting case is the weak-confinement limit, $R/a \gg 1$, for a long polymer $a \ll L$. According to the statistics of a confined Gaussian chain, we expect³¹

$$\beta F = \frac{L}{a} \left[A' \left(\frac{a}{R} \right)^2 + \dots \right] \quad (3)$$

where A' is a different numerical coefficient, although the power law has the same scaling exponent. On average, $\langle r \rangle$ is now a fraction of R ,

$$\frac{\langle r \rangle}{R} = \alpha' \quad (4)$$

where α' is another universal coefficient. While both expressions, eqn (1) and (3), have a similar structure, however, in the crossover region between these two limits, these power laws are no longer valid.

Our theoretical approach in this paper is based on the wormlike-chain formalism in continuum notation.² The calculation of the probability distribution function is mapped into solving a modified diffusion equation, which can then be tackled analytically and numerically. As is shown in Section 3.2,

^aDepartment of Macromolecular Science, Fudan University, Shanghai 200433, China. E-mail: pingtang@fudan.edu.cn; Tel: +86-21-65642867

^bDepartment of Physics and Astronomy, University of Waterloo, Ontario N2L 3G1, Canada. E-mail: jeffchen@uwaterloo.ca; Tel: +1-5198884567-35361

the wormlike-chain formalism analytically reproduces the Gaussian-chain formalism in the weak confinement limit; the prefactor A' can be calculated from the Gaussian-chain confinement problem, discussed in Section 2. Once the density profile is calculated, the calculation of α' becomes trivial.

Morrison and Thirumalai suggested $A_{\text{MTh}} = 0.28$ for the spherical-confinement problem ($D = 3$) on the basis of their numerical calculation.²⁶ As we will demonstrate in Section 3.4, in the asymptotic $R/a \ll 1$ limit, A is exactly the bending energy of a wormlike polymer segment confined on the surface of the confining sphere; for both $D = 2$ and $D = 3$, A can then be analytically determined as well. In the case of $D = 3$, for example, $A = 1/4$, which is an exact solution different from A_{MTh} . Our numerical calculation in Section 3.3 verifies this exact result and further predicts the value for α .

Both asymptotic power laws, eqn (1) and (3), are plotted as green dashed and red solid lines in Fig. 1, respectively. All numerical coefficients determined from this work are summarized in Table 1.

For a long polymer ($L/a \gg 1$), over the entire R/a regime the scaling behavior

$$\beta F = \frac{L}{a} \mu \left(\frac{R}{a} \right) \quad (5)$$

is generally expected, where $\mu(\xi)$ is a crossover function. The wormlike formalism allows us to determine this function numerically, as will be discussed in Section 3. The numerical solution is given in Fig. 1 by circles for both $D = 3$ and $D = 2$. The numerical data is well-represented by an empirical function,

$$\mu = \left(\frac{a}{R} \right)^2 \frac{(A')(R/a)^6 + a_1(R/a)^4 + a_3(R/a)^2 + (A)a_5}{(R/a)^6 + a_2(R/a)^4 + a_4(R/a)^2 + a_5} \quad (6)$$

where the numerical coefficients a_1 to a_5 were obtained from fitting the above expression to the numerical data. The values are given in Table 1. In the three dimensional case, Smyda and Harvey recently studied a discretized wormlike chain model using a Monte Carlo method and produced the value for μ in the mid- to high- R/a range. Their numerical data is represented by squares in Fig. 1(a) and is in agreement with our results represented by circles, in most of the region.

Our numerical solution for the density profile in Section 3 gives us the entire $\langle r \rangle/R$ curve as a function of R/a . The numerical data can be well captured by the empirical expression,

$$\frac{\langle r \rangle}{R} = \frac{1 + b_1(R/a) + b_3(R/a)^2 + \alpha' b_5(R/a)^3}{1 + b_2(R/a) + b_4(R/a)^2 + b_5(R/a)^3} \quad (7)$$

where the coefficients b_1 to b_5 are fitted constants that are listed in Table 1. In the small- R/a limit, we can thus obtain the constant α , which enters in the same table.

The theoretical procedure taken in the current work is based on the ground-state dominating approximation, which is valid for a long wormlike chain polymer, where $L \gg R$ and $L \gg a$. One can show that the modified diffusion equation that the probability function satisfies can be converted into an eigen problem, which requires finding μ as the eigenvalue of an

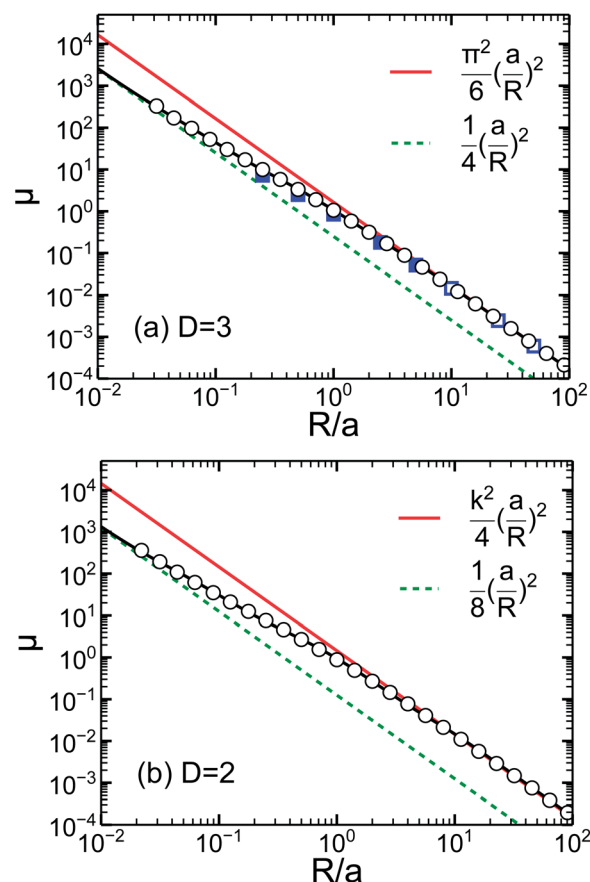


Fig. 1 Reduced free energy per Kuhn segment a , $\mu(R/a)$, defined in eqn (5) for (a) a three-dimensional wormlike chain confined in a spherical cavity of radius R and (b) a two-dimensional wormlike chain confined inside a circle of radius R . Circles represent the numerical solution obtained in this work from finding the partition function. The asymptotic limits of the free energy, in both $R/a \gg 1$ and $R/a \ll 1$ regions, are analytically determined in Section 3.2 and 3.4, and plotted as the red solid and green dashed lines. The black solid line behind the circles represents the empirical expression in eqn (6) with numerical coefficients listed in Table 1. The Monte Carlo simulation results calculated by Smyda and Harvey are plotted as squares for comparison; filled squares were calculated from a discretized wormlike chain model and open squares were calculated from the freely rotating chain model.²⁸

Table 1 Coefficients of the asymptotic power laws in eqn (1)–(4) and constants in the empirical representations, eqn (6) and (7), determined in the current work, where k is the first root of the zeroth-order Bessel function $J_0(k) = 0$. The coefficients A , A' and α' were determined analytically and validated numerically; α was determined from the empirical expression, $\alpha = b_2 - b_1$. We have determined these values for both spherical confinement of a three-dimensional polymer ($D = 3$) and circular confinement of a two-dimensional polymer ($D = 2$)

	$D = 3$	$D = 2$		$D = 3$	$D = 2$
A	1/4	1/8	α	2.266	4.132
A'	$\pi^2/6$	$k^2/4$	α'	1/2	0.4240...
a_1	15.82	5.170	b_1	17.62	−6.002
a_2	13.79	6.213	b_2	19.88	−1.870
a_3	1.229	0.1512	b_3	21.80	137.3
a_4	2.711	0.6065	b_4	46.41	95.94
a_5	0.006618	0.0005571	b_5	−4.507	410.1

operator. This method was successfully used in studying the scaling behavior of the wormlike-chain free energy in slit confinement^{6,32} and most recently, in circular-tube confinement.²¹ The numerical approach taken in this work basically adopts the strategy used in ref. 21. The numerical scheme, however, needs to be carefully redesigned for the current problem, in which a different set of expansion bases needs to be invoked. These are all discussed in Appendix A.

Most of this paper is written in such a way that the dimensionality of space, D , is explicitly maintained in the theory. In this paper we are only interested in two cases, $D = 3$ for a three-dimensional polymer confined in a sphere and $D = 2$ for a two-dimensional polymer confined inside a circle; however, the D -dependence of the formalism gives us a broader horizon beyond these two specific cases.

2 Gaussian chain in spherical confinement

To start, we review the confinement free energy and chain conformation determined from a Gaussian-chain model, which also serves as the weak-confinement limit later in the current paper. Consider a polymer chain of total contour length L with one end labeled $s = 0$ and the other end $s = L$. The spatial coordinates of the monomer located at s are represented by the vector $\mathbf{r}(s)$ in a D -dimensional space. For a given configuration, $\mathbf{r}(s)$, The statistical weight is given by³

$$P[\mathbf{r}(s)] \propto \exp\{-\beta H[\mathbf{r}(s)]\} \quad (8)$$

where within the Gaussian model,

$$\beta H = \frac{D}{2a} \int_0^L ds \left| \frac{d\mathbf{r}(s)}{ds} \right|^2, \quad (9)$$

where a is the Kuhn length. We have explicitly maintained D in the formalism so that the mean-square end-to-end distance $\langle R^2 \rangle$ is always

$$\langle R^2 \rangle = La \quad (10)$$

in a D -dimensional space.

The so-called propagator $G(\mathbf{r}, s)$ is a probability function of finding a polymer segment of length s with the s terminal end appearing at a space point represented by \mathbf{r} . One can show, on the basis of the above distribution function, that it satisfies a modified diffusion equation (MDE)³

$$\frac{\partial}{\partial s} G(\mathbf{r}, s) = \frac{a}{2D} \nabla^2 G(\mathbf{r}, s) \quad (11)$$

where an initial condition, $G(\mathbf{r}, 0) = 1$, must be supplemented for this partial differential equation. Taking advantage of the spherical symmetry in a spherical confinement problem, we consider that the function $G(\mathbf{r}, s)$ can be directly written as $G(r, s)$ where r is the distance from the sphere's center. We then need to solve

$$\frac{\partial}{\partial s} G(r, s) = \frac{a}{2D} \frac{1}{r^{D-1}} \frac{\partial}{\partial r} r^{D-1} \frac{\partial}{\partial r} G(r, s) \quad (12)$$

with the consideration of the boundary conditions

$$\left. \frac{\partial G(r, s)}{\partial r} \right|_{r=0} = G(r, s)|_{r=R} = 0, \quad (13)$$

for any $s \neq 0$. The partition function of the chain can be calculated from

$$Q = \int d\mathbf{r} G(\mathbf{r}, s = L) \quad (14)$$

where the integral covers the interior of the confining sphere.

For a long polymer ($L/a \gg 1$), we can use the ground-state-dominating (GSD) approximation,³³ which assumes

$$G(r, s) = \exp(-\mu s/a) \Psi_0(r) + \dots \quad (15)$$

Thus the reduced free energy is

$$\beta F = -\ln Q = (L/a)\mu + \dots \quad (16)$$

The central focus is finding μ , the reduced free energy per monomer, or chemical potential, of the system.

To find μ we substitute eqn (15) into (12) and rescale r by $\tilde{r} = r/R$. Then, we can write

$$-A' \Psi_0(\tilde{r}) = \frac{1}{2D} \frac{1}{\tilde{r}^{D-1}} \frac{\partial}{\partial \tilde{r}} \tilde{r}^{D-1} \frac{\partial}{\partial \tilde{r}} \Psi_0(\tilde{r}). \quad (17)$$

where

$$\mu \equiv A' \frac{a^2}{R^2}. \quad (18)$$

Hence, A' and $\Psi_0(\tilde{r})$ are the eigenvalue and eigenfunction of the operator on the right-hand side of eqn (17). The boundary conditions are $d\Psi_0/d\tilde{r}(\tilde{r} = 0) = \Psi_0(\tilde{r} = 1) = 0$.

For the problem of a three-dimensional polymer confined inside a spherical cavity of radius R , $D = 3$. Solving the eigen problem analytically, we can show that the eigenfunction is the zeroth-order spherical Bessel function,

$$\Psi_0(\tilde{r}) = B \frac{\sin(\pi \tilde{r})}{\tilde{r}}, \quad (19)$$

and

$$A' = \frac{\pi^2}{6}, \quad (D = 3), \quad (20)$$

where B is a constant.

For the problem of a two-dimensional polymer confined inside a circle of radius R , $D = 2$. Solving the eigen problem analytically, we can show that the eigenfunction is the zeroth-order Bessel function

$$\Psi_0(\tilde{r}) = B J_0(k\tilde{r}) \quad (21)$$

where $k = 2.404826\dots$ is the first root of $J_0(k) = 0$ and B is a constant. The eigenvalue is related to k by

$$A' = k^2/4 = 1.4458\dots \quad (D = 2) \quad (22)$$

Within the GSD approximation, the monomer density is related to the eigenfunction $\Psi_0(\tilde{r})$ by³³

$$\rho(\vec{r}) = \Psi_0^2(\vec{r}). \quad (23)$$

Normalizing the density distribution,

$$\int_0^1 d\tilde{r} \tilde{r}^{D-1} \rho(\tilde{r}) = 1, \quad (24)$$

we can determine the coefficient B in eqn (19) and (21). Thus,

$$\rho(\tilde{r}) = 2 \left[\frac{\sin(\pi\tilde{r})}{\tilde{r}} \right]^2 \quad (25)$$

for $D = 3$ and

$$\rho(\tilde{r}) = \frac{2}{J_1^2(k)} J_0^2(k\tilde{r}) \quad (26)$$

for $D = 2$, where $1/J_1^2(k) = 3.7103\dots$. These results will be compared with the weak-confinement limit of the wormlike chain formalism introduced below.

Finally, we can determine the average monomer distance from the center, from

$$\langle \tilde{r} \rangle = \frac{\langle r \rangle}{R} = \int_0^1 d\tilde{r} \rho(\tilde{r}) \tilde{r}^D. \quad (27)$$

For $D = 3$, we have

$$\frac{\langle r \rangle}{R} = \frac{1}{2} \quad (28)$$

and for $D = 2$, we have

$$\frac{\langle r \rangle}{R} = 0.4240\dots \quad (29)$$

These values enter into Table 1 as the parameter α' .

3 Wormlike chain in spherical confinement

3.1 Model

In this section, we consider a continuous wormlike chain, whose configuration is described by a space curve $\mathbf{r}(s)$, identical to the initial setup in the last subsection. The probability function depends on the tangent vector $\mathbf{u}(s) \equiv d\mathbf{r}(s)/ds$; in this paper we assume that the polymer model is an inextensible thread² such that $|\mathbf{u}(s)| = 1$, although some models for semiflexible chains relax this constraint.^{2,34–37}

According to Saito–Takahashi–Yunoki, for a wormlike chain the statistical weight in eqn (8) is associated with a bending energy²

$$\beta H = \frac{\beta\epsilon}{2} \int_0^L ds \left| \frac{d\mathbf{u}(s)}{ds} \right|^2 \quad (30)$$

where $\beta\epsilon$ is the bending energy modulus reduced by the inverse temperature β . The connection between $\beta\epsilon$ and the persistence length can be found by considering the orientational correlation function.

Assume that the monomer at $s = 0$ has a tangent vector $\mathbf{u}'(0)$ and the monomer at s has a tangent vector $\mathbf{u}(s)$. Defining $\mathbf{u}(s) \cdot \mathbf{u}'(0) = \cos \theta$, we need to solve²

$$\frac{\partial G}{\partial s} = \frac{1}{2\beta\epsilon} \frac{1}{\sin^{D-2} \theta} \frac{\partial}{\partial \theta} \sin^{D-2} \theta \frac{\partial G}{\partial \theta} \quad (31)$$

for the Green's function $G(\theta, s)$ in D dimensions. The solution that satisfies the initial condition

$$G(\theta, 0) = \delta(\theta) \quad (32)$$

is

$$G(\theta, s) = \sum_n \exp[-n(n+D-2)s/2\beta\epsilon] C_n(\cos \theta) C_n(1) / R_n^2 \quad (33)$$

where $C_n(x)$ is the Gegenbauer polynomial of degree n in D -dimensional space,³⁸ an abbreviation of the original notation $\equiv C_n^{(D/2-1)}(x)$, and

$$R_n^2 = \int_0^\pi [C_n(\cos \theta)]^2 \sin^{D-2} \theta d\theta. \quad (34)$$

Making use of the orthonormal properties of the Gegenbauer polynomials, we find

$$\langle \mathbf{u}(s) \cdot \mathbf{u}'(0) \rangle = \int_0^\pi \cos \theta G(\theta, s) \sin^{D-2} \theta d\theta = e^{-(D-1)s/2\beta\epsilon}. \quad (35)$$

Thus, in D -dimensions, the orientation–orientation correlation length, or the *persistence length*, is given by

$$\lambda = 2\beta\epsilon/(D-1). \quad (36)$$

Consequently we can rewrite the reduced bending energy

$$\beta H = \frac{(D-1)\lambda}{4} \int_0^L ds \left| \frac{d\mathbf{u}(s)}{ds} \right|^2 \quad (37)$$

in a D -dimensional space.^{39,40}

Similar to the procedure used in dealing with a Gaussian chain, now we introduce a propagator $q(\mathbf{r}, \mathbf{u}; s)$, which represents the probability of finding a polymer segment of length s with its terminal end appearing at a space point represented by the vector \mathbf{r} and pointing at the direction specified by the unit vector \mathbf{u} ; the partition function Q can be obtained from

$$Q = \int d\mathbf{r} d\mathbf{u} q(\mathbf{r}, \mathbf{u}; L). \quad (38)$$

Rather than integrating over the probability function, a mathematically equivalent procedure of finding $q(\mathbf{r}, \mathbf{u}, s)$ is solving the MDE,^{2,34,41}

$$\frac{\partial}{\partial s} q(\mathbf{r}, \mathbf{u}; s) = \left\{ -\mathbf{u} \cdot \nabla_{\mathbf{r}} + \frac{1}{(D-1)\lambda} \nabla_{\mathbf{u}}^2 + [(\mathbf{u} \cdot \nabla_{\mathbf{r}}) \mathbf{u}] \cdot \nabla_{\mathbf{u}} \right\} q(\mathbf{r}, \mathbf{u}; s). \quad (39)$$

The last term, which vanishes in a Cartesian coordinate system, is an explicit consideration for a curvilinear coordinate system which requires a non-trivial modification to the MDE.⁴¹ The solution to this partial differential equation is subject to the initial condition $q(\mathbf{r}, \mathbf{u}; 0) = 1$ and appropriate boundary conditions for a confined system.

3.2 The weak-confinement limit $R/\lambda \gg 1$

Consider the typical length scale in the system, which in our case is the hyperspherical radius R . We can analytically show that the MDE for a wormlike chain in eqn (39) recovers the MDE for a Gaussian chain in eqn (11) in the limit of $R/\lambda \gg 1$ and $L/\lambda \gg 1$ for a D -dimensional chain.

The proof is similar to the one presented in Appendix B of ref. 42 for a $D = 3$ system. It is most convenient to consider the proof in the Cartesian coordinate system where the last term on the right-hand side of eqn (39) disappears. After transforming $q(\mathbf{r}, \mathbf{u}; s)$ to its Fourier transformation $I(\mathbf{k}, \mathbf{u}; s)$ where \mathbf{k} is the wave vector, we have

$$\frac{\partial}{\partial s} I(\mathbf{k}, \mathbf{u}; s) = \left[\frac{1}{(D-1)\lambda} \nabla_{\mathbf{u}}^2 + i\mathbf{u} \cdot \mathbf{k} \right] I(\mathbf{k}, \mathbf{u}; s). \quad (40)$$

Defining $\mathbf{u} \cdot \mathbf{k} = k \cos \theta$ where $k = |\mathbf{k}|$ and expanding the function $I(\mathbf{k}, \mathbf{u}; s)$ in terms of the Gegenbauer polynomials $C_n(\cos \theta)$, we have

$$I(\mathbf{k}, \mathbf{u}; s) = \sum_n \gamma_n(k; s) C_n(\cos \theta) / R_n. \quad (41)$$

Plugging this expansion in eqn (40) and using the recursion relation of the Gegenbauer polynomial, we arrive at

$$\begin{aligned} \lambda \frac{\partial}{\partial s} \gamma_n(k; s) = & -\frac{n(n+D-2)}{(D-1)} \gamma_n(k; s) \\ & + ik\lambda \left[\frac{n+1}{(2n+D-2)} R_{n+1}^2 \gamma_{n+1}(k; s) \right. \\ & \left. + \frac{n+D-3}{(2n+D-2)} R_{n-1}^2 \gamma_{n-1}(k; s) \right] / R_n^2, \end{aligned} \quad (42)$$

for any $n \geq 1$. For $n = 0$, the first and last terms in the above expression vanish. For the purpose of dealing with the $R/\lambda \gg 1$ limit, it is adequate to consider the $k\lambda \ll 1$ regime. Comparing the first and last terms on the right-hand side, we conclude that the function $\gamma_n(k; s)$ has a leading order $(k\lambda)^n$. Consequently, taking $n = 0$ we have

$$\lambda \frac{\partial}{\partial s} \gamma_0(k; s) = \frac{ik\lambda R_1^2}{(D-2)R_0^2} \gamma_1(k; s), \quad (43)$$

which shows that the effect of the operator $\lambda \partial/\partial s$ corresponds to an order $(k\lambda)^2$. Keeping this in mind, we take $n = 1$ and obtain

$$\mathcal{O}(k\lambda)^3 = -\gamma_1(k; s) + ik\lambda \left[\mathcal{O}(k\lambda)^2 + \frac{D-2}{D} R_0^2 \gamma_0(k; s) \right] / R_1^2. \quad (44)$$

Combining the two equations yields

$$\lambda \frac{\partial}{\partial s} \gamma_0(k; s) = -\frac{(k\lambda)^2}{D} \gamma_0(k; s) + \mathcal{O}(k\lambda)^4, \quad (45)$$

In the \mathbf{r} space, we have

$$\frac{\partial}{\partial s} q_0(\mathbf{r}; s) = \frac{\lambda}{D} \nabla_{\mathbf{r}}^2 q_0(\mathbf{r}; s), \quad (46)$$

where

$$q_0(\mathbf{r}; s) = \int q(\mathbf{r}, \mathbf{u}; s) d\mathbf{u} / \Omega_D \quad (47)$$

and Ω_D is the total solid angle in the D -dimensional space.

This equation is identical to the MDE, eqn (11), for the Gaussian-chain problem, as long as we link λ with a ,

$$a = 2\lambda, \quad (48)$$

which is an identification generally valid in a D -dimensional problem. In the remainder of this paper, we directly use a instead of λ through this connection.

When we arrived at eqn (45), we stated that from an order-of-magnitude point of view, $\lambda \partial/\partial s \sim (k\lambda)^2$. Realizing that $s = [0, L]$, we rewrite this condition as $\lambda/L \sim (\lambda/R)^2$. Hence, the recovery of the Gaussian-chain MDE from the wormlike-chain MDE is accompanied by the condition

$$L/a \sim (R/a)^2 \gg 1 \quad (49)$$

as well.

We directly use the analytic A' and α' calculated in Section 2, shown in eqn (20), (22), (28) and (29) which are listed in Table 1 for the current wormlike-chain model. As we will see below, these *analytic* results are validated as the limiting case by the *numerical* solution obtained over the entire R/a regime.

3.3 D -dimensional wormlike chain confined in a hyperspherical cavity

We return to the general discussion of the propagator $q(\mathbf{r}, \mathbf{u}; s)$ which satisfies the MDE, eqn (39). To solve the spherical-confinement problem, we use a coordinate system centered at the hypersphere's center. Due to the spherical symmetry, the current problem inherently only has dependence on the distance from the sphere's center, r , and the angle that \mathbf{u} makes with respect to \mathbf{r} , namely θ . For example, in $D = 2$ and $D = 3$ systems, we can identify these two variables as illustrated in Fig. 2. Using this symmetry property, we can greatly simplify the MDE.

We are interested in the case where the polymer is much longer than both R and a . Therefore, we can take the GSD approximation for the propagator,³³

$$q(\mathbf{r}, \mathbf{u}; s) = \exp(-\mu s/a) \Psi_0(\tilde{r}, \theta) + \dots \quad (50)$$

Thus, the MDE is converted to

$$\begin{aligned} \left[\frac{2}{D-1} \frac{1}{\sin^{D-2} \theta} \frac{\partial}{\partial \theta} \left(\sin^{D-2} \theta \frac{\partial}{\partial \theta} \right) - \frac{a}{R} \cos \theta \frac{\partial}{\partial \tilde{r}} \right. \\ \left. + \frac{a}{R} \frac{\sin \theta}{\tilde{r}} \frac{\partial}{\partial \theta} \right] \Psi_0(\tilde{r}, \theta) = -\mu \Psi_0(\tilde{r}, \theta) \end{aligned} \quad (51)$$

where μ and Ψ_0 are the ground-state eigenvalue and eigenfunction, respectively. The solution depends on the ratio R/a . Thus the free energy of the system is

$$\beta F = \mu L/a + \dots \quad (52)$$

This problem is accompanied by the natural boundary conditions

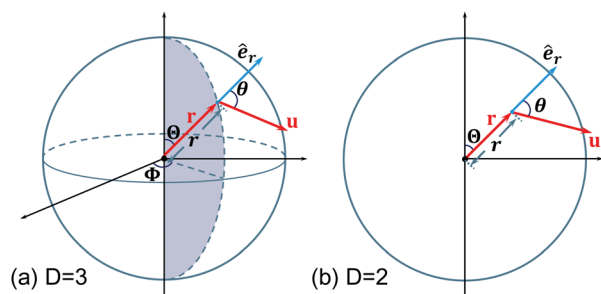


Fig. 2 Examples of the coordinate systems used in this work: (a) $D = 3$ and (b) $D = 2$. The probability distribution function $q(r, \mathbf{u}; s)$ depends on both r, \mathbf{u} , illustrated by the red vectors in the figure. In three dimensions, within the spherical coordinate system, at the point specified by r , a vector basis set, $\hat{e}_r, \hat{e}_\theta$ and \hat{e}_ϕ can be defined;⁴³ In reference to \hat{e}_r , a polar variable θ is defined to specify \mathbf{u} . In two dimensions, within a polar coordinate system, at the point specified by r , a vector basis set, \hat{e}_r and \hat{e}_θ can be defined;⁴³ In reference to \hat{e}_r , a polar variable θ is defined to specify \mathbf{u} .

$$\left. \frac{\partial}{\partial \theta} \Psi_0(\tilde{r}, \theta) \right|_{\tilde{r}=0} = 0, \quad (53)$$

$$\left. \frac{\partial}{\partial \tilde{r}} \Psi_0(\tilde{r}, \theta) \right|_{\tilde{r}=0} = 0, \quad (54)$$

and

$$\left. \frac{\partial}{\partial \theta} \Psi_0(\tilde{r}, \theta) \right|_{\theta=0, \pi} = 0. \quad (55)$$

The specification of the boundary condition at $\tilde{r} = 1$ follows the fact that a chain end pointing in a direction within the range $\theta = [0, \pi/2]$ is allowed and otherwise disallowed

$$\Psi_0(\tilde{r} = 1, \theta) = 0, \text{ if } \theta > \pi/2. \quad (56)$$

Similar conditions were used for various related systems where the presence of a confinement hard wall requires a \mathbf{u} -dependent boundary condition.^{6,21,44,45}

In Appendix A we outline a numerical procedure that can be used to solve this eigen problem. For each given value of R/a we must carry out the eigenvalue–eigenfunction calculation through an iterative procedure. The resulting μ for a set of R/a is displayed by circles in Fig. 1 and listed in Table 2, covering a significant range of R/a . In the large R/a limit, the data approaches the analytically asymptotic limit in eqn (20), which is plotted in Fig. 1 as the straight solid line.

The numerical data calculated by Smyda and Harvey²⁸ using Monte Carlo techniques for $D = 3$ is plotted as squares in Fig. 1(a). In the high R/a regime, the data from the current study and ref. 28 agrees well; as matter of fact, the data associated with the open squares were simulated using a freely-rotating chain model rather than the wormlike chain model. In the mid R/a regime, the two sets of data begin to deviate; this can be attributed to the fact that the wormlike chain model used by Smyda and Harvey is a discrete version of the continuum model considered here in eqn (30). In an idealized discrete model, the length of the straight polymer segment should be much less

Table 2 The free energy per segment, $\mu(R/a) \equiv \beta a L^{-1} F(R/a)$, determined in this work over a wide range of R/a for a long wormlike chain, $a/L \ll 1$ and $R \ll L$. The data were numerically calculated from systems where the ranges of the angle θ and variable \tilde{r} were divided into M and N representative nodes. $N = 80$ and $M = 401$ were used in this calculation

R/a	$\mu(R/a)$		R/a	$\mu(R/a)$	
	$D = 3$	$D = 2$		$D = 3$	$D = 2$
2^{-5}	327.4	192.7	$2^{0.5}$	0.5813	0.4919
$2^{-4.5}$	178.3	108.6	2^1	0.3146	0.2696
2^{-4}	97.17	61.57	$2^{1.5}$	0.1678	0.1456
$2^{-3.5}$	52.76	35.02	2^2	0.0883	0.07745
2^{-3}	30.20	20.98	$2^{2.5}$	0.04596	0.04073
$2^{-2.5}$	17.11	12.52	2^3	0.02368	0.02060
2^{-2}	9.986	7.629	$2^{3.5}$	0.01213	0.01097
$2^{-1.5}$	5.790	4.567	2^4	0.006155	0.005385
2^{-1}	3.331	2.688	$2^{4.5}$	0.003125	0.002889
$2^{-0.5}$	1.892	1.554	2^5	0.001579	0.001380
2^0	1.057	0.8817	2^6	0.0007961	0.0007530

than the confining radius. In actual implementation, near the strong confinement regime the finite length of such a segment starts to display finite-size effects on top of the properties described by a continuum model.

The numerical solution to the MDE allows us to calculate the monomer density distribution profile, normalized to unity,

$$\rho(\tilde{r}) = \frac{\int_0^\pi \Psi_0(\tilde{r}, \theta) \Psi_0(\tilde{r}, \pi - \theta) \sin^{D-2} \theta d\theta}{\int_0^1 \int_0^\pi \Psi_0(\tilde{r}, \theta) \Psi_0(\tilde{r}, \pi - \theta) \tilde{r}^{D-1} \sin^{D-2} \theta d\tilde{r} d\theta}. \quad (57)$$

We display the data in Fig. 3 using two methods. Density plots were made in Fig. 3(a) and (b) to visualize the density variation over the confined region. The function $\rho(\tilde{r})$ itself is plotted in Fig. 3(c) and (d) for various values of R/a . In the $R/a \gg 1$ limit, the density profile approaches the asymptotic behavior, determined from the Gaussian model, illustrated by the black curve in the figure; most polymer segments are located near the central region, staying away from the confining wall. On the other hand, in the $R/a \ll 1$ limit, the wormlike chain seeks a configuration that allows for the minimum cost of the bending energy; the entire polymer wraps around the interior wall surface of the confinement cavity. When the radius is significantly smaller than a , a thin concentrated layer forms near the edge of the spherical shell. This result is consistent with recent experimental observations.^{46,47}

On the basis of $\rho(\tilde{r})$, we can then evaluate the average monomer distance from the center,

$$\langle r \rangle / R = \int_0^1 \rho(\tilde{r}) \tilde{r}^D d\tilde{r} \quad (58)$$

for various R/a . The numerical results are plotted in Fig. 4 in a semilogarithmic plot; also shown in the figure, is the fitted empirical formula, eqn (7), which is plotted as the solid curve behind the symbols.

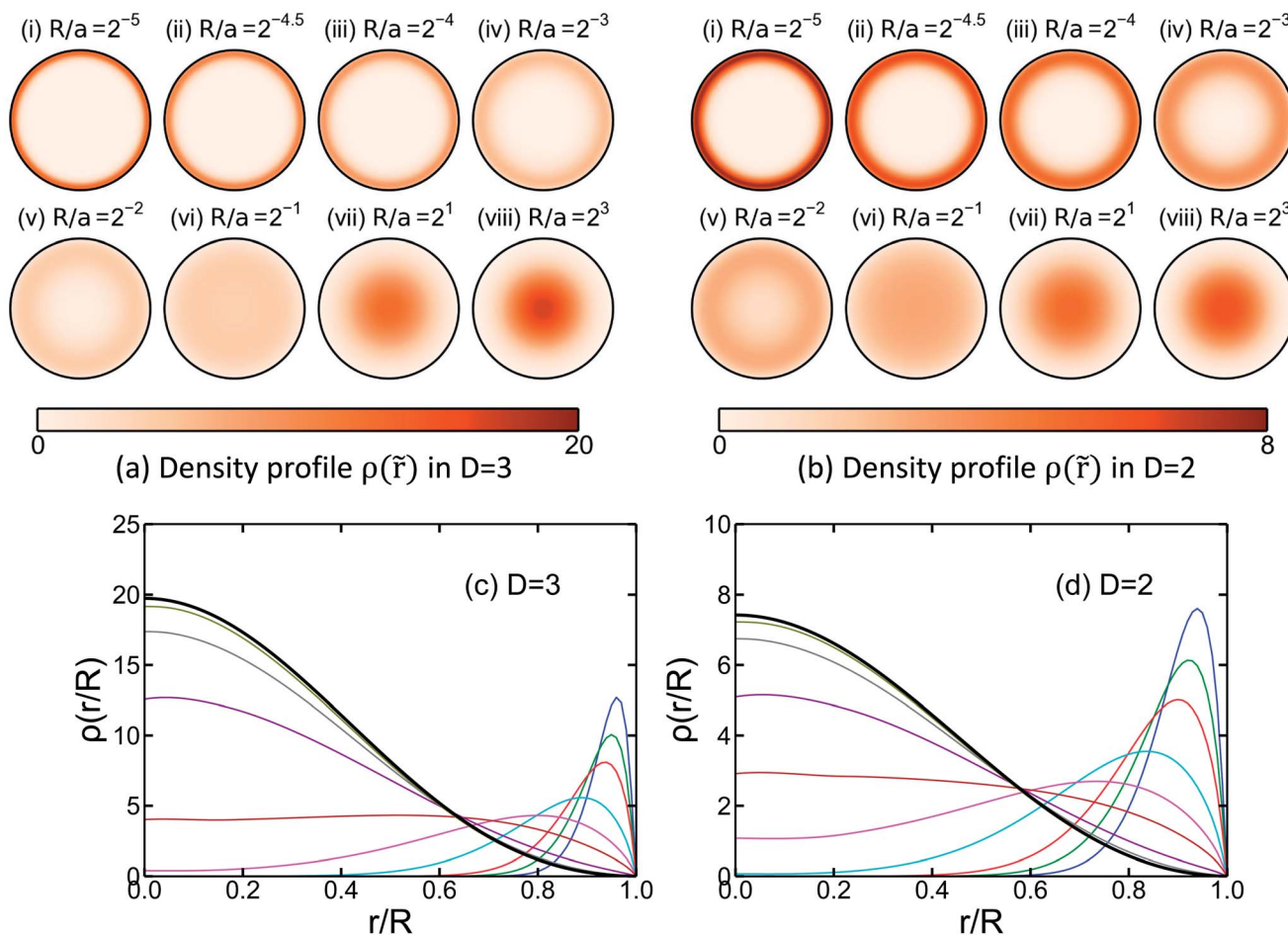


Fig. 3 Normalized density-profile plots for a three-dimensional ($D = 3$) and two-dimensional ($D = 2$) wormlike chain confined inside a spherical cavity and circle, respectively. In (a) and (b), the density is shown by grey scale for systems having the radius/Kuhn length ratio (i) $R/a = 2^{-5}$, (ii) $2^{-4.5}$, (iii) 2^{-4} , (iv) 2^{-3} , (v) 2^{-2} , (vi) 2^{-1} , (vii) 2 , and (viii) 2^3 . The low- to high-density regions are represented by the light to dark colors respectively. In (c) and (d), the density is shown as a function of r/R for $R/a = 2^{-5}$ (blue), $2^{-4.5}$ (green), 2^{-4} (red), 2^{-3} (cyan), 2^{-2} (magenta), 2^{-1} (brown), 2 (purple), 2^3 (gray), and 2^6 (olive). In addition, we have plotted the Gaussian-chain density, eqn (25) and (26) for $D = 3$ and $D = 2$ respectively, as the black curve.

The wormlike-chain formalism deals with directional ordering in the system as a variable. Near the wall the polymer segments make a parallel arrangement with the wall surface, excluded from the hard-wall confinement. To visualize the orientational order in the system, we examine the order-parameter profile,

$$S(\tilde{r}) = \frac{\int_0^\pi \Psi_0(\tilde{r}, \theta) \Psi_0(\tilde{r}, \pi - \theta) \left[(3\cos^2 \theta - 1)/2 \right] \sin \theta d\theta}{\int_0^\pi \Psi_0(\tilde{r}, \theta) \Psi_0(\tilde{r}, \pi - \theta) \sin \theta d\theta} \quad (59)$$

for $D = 3$, and the order-parameter profile

$$S(\tilde{r}) = \frac{\int_0^{2\pi} \Psi_0(\tilde{r}, \theta) \Psi_0(\tilde{r}, \pi - \theta) (\cos 2\theta) d\theta}{\int_0^{2\pi} \Psi_0(\tilde{r}, \theta) \Psi_0(\tilde{r}, \pi - \theta) d\theta} \quad (60)$$

for $D = 2$ in Fig. 5. These definitions are consistent with those defined in a liquid-crystal system in both dimensions. A value of $S = -1/2$ or a value of $S = -1$ in $D = 3$ or $D = 2$, for example,

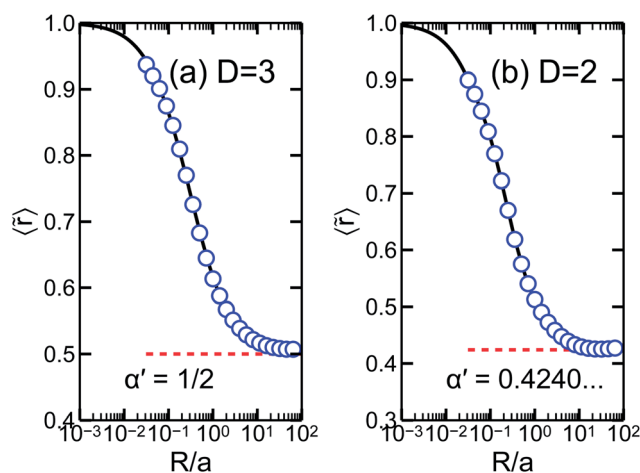


Fig. 4 Average monomer-to-center distance, $\langle r \rangle / R$, as a function of R/a for (a) $D = 3$ and (b) $D = 2$ in the full R/a range. The asymptotic limit in large R/a is $\langle \tilde{r} \rangle = \alpha'$ as defined in eqn (2), where $\alpha' = 1/2$ for $D = 3$, and $0.4240...$ for $D = 2$, both listed in Table 1.

characterizes the perfect alignment of the polymer segment along a direction perpendicular to \hat{e}_r (*i.e.*, $\theta = \pi/2$). In Fig. 5(a) and (b), we present density plots of $S(\tilde{r})$ and in Fig. 5(c) and (d), we plot the function $S(\tilde{r})$ itself, for various values of R/a of interest in this paper, over the entire region of confinement. In the weak-confinement region when $R/a \gg 1$, most polymer segments display orientational disorderness $S = 0$ in the central region where the segment density is the highest. From the original function $\Psi_0(\tilde{r}, \theta)$ we can also deduce that orientationally the polymer segments order in parallel with the wall surface near $\tilde{r} = 1$; the polymer density in this region, however, is low; hence the plot for $R/a = 2^3$ displays an overall low magnitude. In the strong confinement region when $R/a \ll 1$, the segment density is high near the confinement wall; the orientational order parameter approaches $-1/2$ for $D = 3$ and -1 for $D = 2$ in this region.

3.4 Strong confinement limit $R/a \ll 1$

In this section we analyze the structure of the MDE in eqn (51), in order to analytically obtain the eigenvalue μ in the strong

confinement limit $R/a \ll 1$. Physically, in this extreme limit, the wormlike chain polymer wrap around the hyperspherical surface. Considering the bending energy alone, from eqn (37) we have

$$\beta F_{\text{bend}} = (D - 1)aL/8R^2. \quad (61)$$

Thus, according to eqn (5),

$$\mu_{\text{bend}} = \frac{D - 1}{8} \left(\frac{a}{R} \right)^2. \quad (62)$$

To validate this argument that the bending energy dominates over the entropic effects, we mathematically deduce from the differential equation in eqn (51) that A yields the same result; this is done below.

We start the discussion with the fact that for $R/a \ll 1$ the density distribution function in Fig. 3 is significant only in the vicinity of $\tilde{r} = 1$. We introduce a new variable ξ instead of \tilde{r} ,

$$\tilde{r} = 1 - C\xi, \quad (63)$$

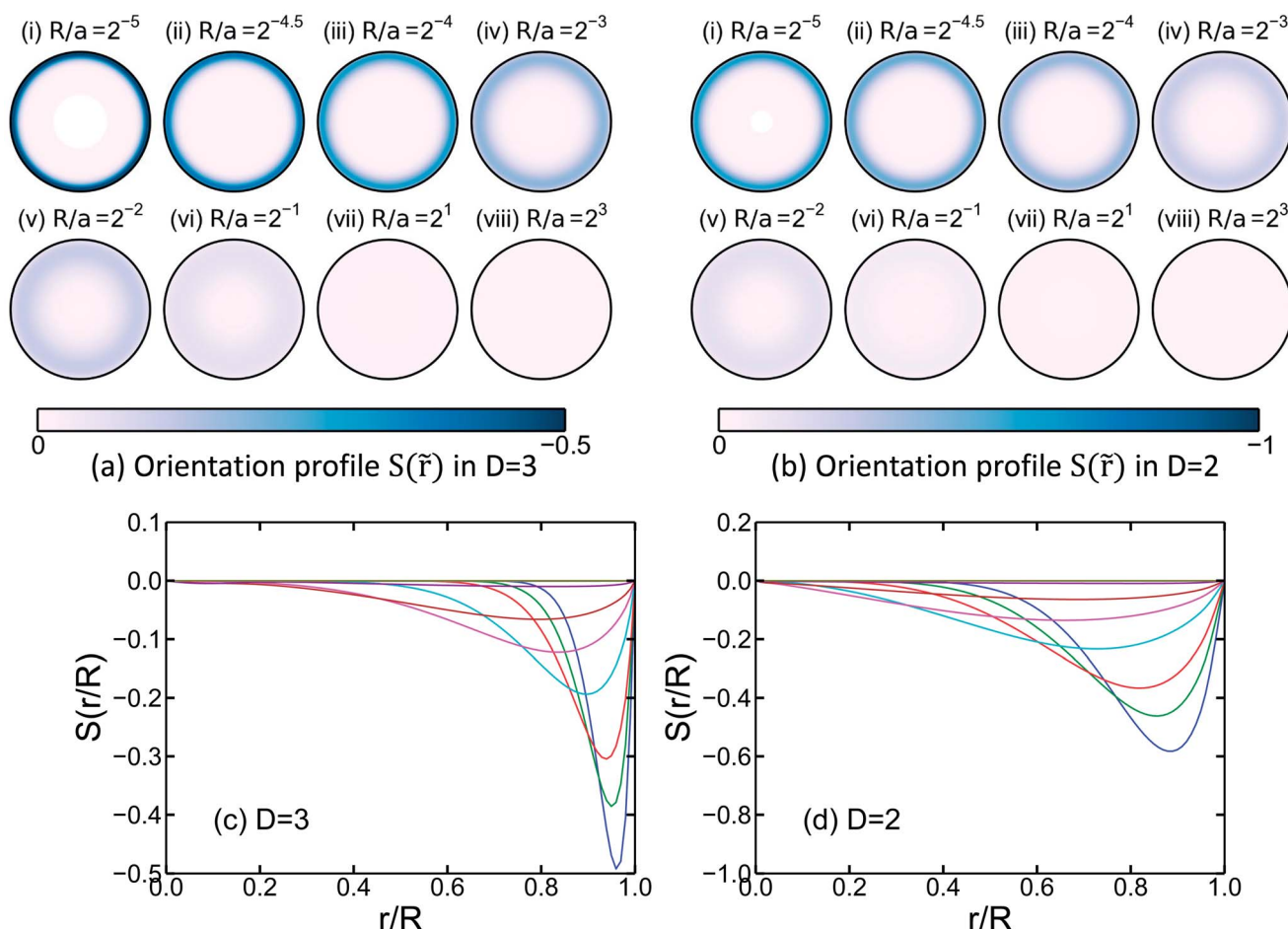


Fig. 5 Orientational order parameter profiles for a three-dimensional ($D = 3$) and two-dimensional ($D = 2$) wormlike polymer confined in a spherical cavity and a circle, respectively. In plots (a) and (b), the order parameter is plotted in a grey scale, for (i) $R/a = 2^{-5}$, (ii) $2^{-4.5}$, (iii) 2^{-4} , (iv) 2^{-3} , (v) 2^{-2} , (vi) 2^{-1} , (vii) 2, and (viii) 2^3 . The low- to high-orientational order regions are represented by light to dark colors. In plots (c) and (d), the order parameter is plotted as a function of r/R , for systems having the radius/Kuhn length ratio $R/a = 2^{-5}$ (blue), $2^{-4.5}$ (green), 2^{-4} (red), 2^{-3} (cyan), 2^{-2} (magenta), 2^{-1} (brown), 2 (purple), 2^3 (gray) and 2^6 (olive). Note that an idealized orientational ordering in $D = 3$ and $D = 2$ has the value $S = -1/2$ and -1 , respectively.

where C is asymptotically small. For the region beyond the immediate vicinity of $\theta = \pi/2$, the MDE in eqn (51) is dominated by

$$\frac{a}{R} \frac{\cos \theta}{C} \frac{\partial}{\partial \xi} \psi(\xi, \theta) = -\mu \psi(\xi, \theta) \quad (64)$$

where

$$\psi(\xi, \theta) = \Psi_0(1 - C\xi, \theta). \quad (65)$$

As we expect $\mu \propto (a/R)^2$, matching the order of magnitude on both sides of the equation, we obtain

$$C = R/a. \quad (66)$$

Therefore, we draw our first conclusion on the scaling relation

$$\langle \tilde{r} \rangle = 1 - \alpha R/a + \dots \quad (67)$$

in the asymptotic limit $R/a \ll 1$. The constant α appears in eqn (2).

Now, near $\theta = \pi/2$, the first and third terms on the left-hand side of eqn (51) become more important than the second term. Taking

$$\theta = \pi/2 - (R/a)\zeta \quad (68)$$

for a moderate ζ , for small R/a we can rewrite eqn (51) as

$$\left[\frac{2}{D-1} \frac{d^2}{d\zeta^2} - \frac{d}{d\zeta} \right] f(\zeta) = -\tilde{\mu} f(\zeta) \quad (69)$$

where

$$f(\zeta) = \Psi_0 \left(1, \frac{\pi}{2} - \frac{R}{a} \zeta \right). \quad (70)$$

and $\mu = A(a/R)^2$. The function has value in the $\zeta > 1$ regime and connects to the boundary condition in eqn (56) by $f(0) = 0$.

There exist two cases for the solution of this second-order linear differential equation. In the first case, $f(\zeta)$ has a formal solution

$$f(\zeta) = c_+ e^{\nu_+ \zeta} + c_- e^{\nu_- \zeta}, \quad (71)$$

where c_{\pm} are constants and ν_{\pm} are non-repeated roots of the characteristic equation

$$\frac{2}{D-1} \nu^2 - \nu = -A, \quad (72)$$

which has the roots

$$\nu_{\pm} = (D-1) \left(1 \pm \sqrt{1 - A/A_{\text{bend}}} \right) / 4 \quad (73)$$

where $A_{\text{bend}} = (D-1)/8$. Note that the expression inside the square root is always negative or zero, because we expect $A \geq A_{\text{bend}}$. The negative value creates an oscillating solution for $f(\zeta)$, which, by the original definition of the partition function, must be positive-definite and cannot be oscillative. Hence, the case of two roots is ruled out.

We are then left with the second case, where the two roots are identical,

$$\nu_0 = (D-1)/4. \quad (74)$$

In this case, we have a general solution

$$f(\zeta) = c_1 e^{\nu_0 \zeta} + c_2 \zeta e^{\nu_0 \zeta}. \quad (75)$$

Upon consideration of the boundary condition, we have $c_1 = 0$ and keep the second term. The requirement of double roots hence yields

$$A = A_{\text{bend}} = (D-1)/8. \quad (76)$$

This completes our analysis of μ in the $R/a \ll 1$ limit.

Therefore, in the extreme case when $R/a \rightarrow 0$, the wormlike chain is pushed to the confining wall and behaves no differently from a chain directly confined on the surface of the sphere ($D = 3$) or the perimeter of the circle ($D = 2$). This paper concerns a long wormlike chain polymer ($L \gg a$ and $L \gg R$) which makes many wrapping turns on the spherical surface and loses the directional correlation after these turns. For a shorter wormlike chain polymer, the correlation between the wrapping turns must be considered as studied by Spakowitz and Wang⁴⁸ for a wormlike chain on a spherical surface and Lin *et al.*⁴⁹ for a wormlike chain on a cylindrical surface.

4 Summary

In summary, through solving the eigenvalue problem of the modified diffusion equation that the probability function of a confined wormlike chain satisfies, we have determined the free energy and conformational properties of a wormlike polymer confined in a spherical cavity, with an explicit dimensionality (D) dependence. The strong- and weak-confinement limits were examined mainly by analytic methods, whereas the crossover region between these two limits was examined by a numerical technique. The computational tactics involved an expansion of the distribution function in terms of the Chebyshev polynomial to deal with the particular boundary conditions for the current problem.

While this paper clarifies the confined wormlike-chain structure according to the standard model in eqn (37), by no means it attempts to address the self-avoiding wormlike-chain problem. The treatment in this paper ignores the excluded-volume interaction between polymer segments. For a qualitative analysis, let us assume that the structure within the sphere can be dissected layer by layer, similar to peeling an onion. In a $R/a \ll 1$ system, the inner core has a low monomer density, but within a layer having a distance $r \sim R^2/a$ away from the outmost layer, a high monomer density is expected. The effective volume occupied by the polymer segments is then $V \sim 4\pi R^2 \times r \sim 4\pi R^4/a$. From earlier work,^{4,39,40,50} we understand that when the reduced density daL/V reaches an approximate magnitude $daL/V \sim 10$, a wormlike segment experiences a high Onsager interaction potential and starts to order orientationally in parallel to the direction of nearby segments, where d is the diameter of a wormlike filament. Hence, when the condition $daL/V \sim Lda^2/4\pi R^4 \sim 10$ is satisfied, near the confinement wall, significant orientational ordering is expected.

Now, the topological frustration between a nematic field and the finite geometry on a spherical surface can produce orientational-order disclinations within these high density layers.^{51–54} In a recent Monte Carlo study of a polyelectrolyte adsorbed on an oppositely charged spherical surface, Angelescu *et al.* indicated that the orientational texture could either be a perfect helicoidal or tennis-ball alike⁵⁵ and further speculated that the electrostatic interaction is the cause of the non perfect helicoidal conformation; in another Monte Carlo study, a wrapped wormlike chain on spherical surface was considered where the excluded-volume effects were modeled by no electrostatic interaction; Zhang and Chen gave a concrete numerical evidence that at relatively high segment densities, the directionally ordered state is a conformation similar to the texture on the tennis-ball surface, not helicoidal.⁵⁶ Hence, it is reasonable to expect that in the self-excluding wormlike-chain confinement problem, the ordered outermost layers near the confinement wall display orientational-order disclinations, similar to those seen in a liquid-crystal problem. Attention to this type of details, however, has not been paid in recent Monte Carlo simulations.^{26,29}

It should be noted that the inclusion of the excluded-volume effects in the current treatment is possible. One can introduce an Onsager-like interaction energy,^{57,58} which in turn shows up as a self-consistent field, to be inserted into eqn (39).⁵⁹ This theoretical treatment is at an approximation level similar to the Flory treatment of the excluded-volume interaction. Then, for a $D = 3$ problem, we must solve a five-variable diffusion equation (three for \mathbf{r} and two for \mathbf{u}) within the ground state dominating approximation that removes the variable s in eqn (39). Although recent progress has been made in solving a similar equation for a periodic structure with all variables presented,^{42,60} the modification of the algorithm for the current problem remains a challenging task.

A Appendix

In this Appendix, we layout the numerical steps used to solve the eigenvalue problem presented in eqn (51) for the three-dimensional case, $D = 3$. The $D = 2$ case can be dealt with in a similar way and thus is not discussed here. The main idea is to use an updating scheme that improves the previous guess for the eigen function $\Psi_{0(\text{old})}(\tilde{r}, \theta)$. An initial guess is needed to implement this scheme.

We treat the entire square brackets on the left-hand side of eqn (51) by separating it into three operators gives

$$\hat{\mathcal{L}}_1 = \frac{1}{\sin \theta} \frac{\partial}{\partial \theta} \left(\sin \theta \frac{\partial}{\partial \theta} \right), \quad (77)$$

$$\hat{\mathcal{L}}_2 = -\frac{a}{R} \cos \theta \frac{\partial}{\partial \tilde{r}}, \quad (78)$$

and

$$\hat{\mathcal{L}}_3 = \frac{a}{R} \frac{\sin \theta}{\tilde{r}} \frac{\partial}{\partial \theta}. \quad (79)$$

We then find a new function, $\Psi_{0(\text{new})}(\tilde{r}, \theta)$, from solving

$$\Psi_{0(\text{new})} = \Psi_{0(\text{old})} + \varepsilon [(\hat{\mathcal{L}}_1 + \hat{\mathcal{L}}_3)\Psi_{0(\text{new})} + \hat{\mathcal{L}}_2\Psi_{0(\text{old})}], \quad (80)$$

where ε is a small parameter. The assumption is that, once the difference $[\Psi_{0(\text{new})} - \Psi_{0(\text{old})}]/\varepsilon$ converges to a constant $-\tilde{\mu}$, we obtain both eigenvalue and eigenfunction.

To deal with the hard-wall boundary condition in eqn (56) properly while enjoying the numerical precision of a spectral method, we use the Chebyshev spectral method^{61,62} rather than the spherical-harmonic based spectral method,⁶⁰ to treat the derivatives on the θ dependence. We divided the range $[0, 1]$ for \tilde{r} into N nodes, \tilde{r}_i , where $i = 1, 2, 3, \dots, N$, and the range $[0, \pi]$ for θ into M nodes, θ_j , where $j = 1, 2, 3, \dots, M$. The node θ_j was adopted such that $\cos \theta_j$ corresponds to the Chebyshev nodes.⁶¹ M is selected to be an odd number. The function Ψ_0 is then represented by a matrix of size NM , $\Phi_{ji} \equiv \Psi_0(\tilde{r}_i, \theta_j)$.

In order to use the Chebyshev spectral method, we employ the Chebyshev differentiation matrix,⁶¹ $\Delta_{jj'}$ where $j, j' = 1, 2, \dots, M$, to represent the derivative with respect to θ . As well, we introduce a tridiagonal $N \times N$ matrix

$$[\bar{\Delta}_{ii'}] = \frac{1}{w_{\tilde{r}}} \begin{bmatrix} -1 & 1 & 0 & \dots & & \\ -1/2 & 0 & -1/2 & 0 & \dots & \\ 0 & -1/2 & 0 & -1/2 & 0 & \dots \\ \dots & \dots & \dots & \dots & \dots & \dots \\ \dots & \dots & 0 & -1/2 & 0 & -1/2 \\ \dots & \dots & \dots & 0 & -1 & 1 \end{bmatrix} \quad (81)$$

to represent the derivative with respect to \tilde{r} , where $w_{\tilde{r}} = 1/(N-1)$ is the weight of each spatial node. Denoting

$$\Delta_{jj'}^2 \equiv \sum_{k=1}^M \Delta_{jk} \Delta_{kj'} \quad (82)$$

as the second-order differentiation operator, we can write

$$[\hat{\mathcal{L}}_1 \Psi_0]_{ji} = \sum_{j'} \left[\Delta_{jj'}^2 + \frac{\cos \theta_j}{\sin \theta_j} \Delta_{jj'} \right] \Phi_{j'i} \quad (83)$$

$$[\hat{\mathcal{L}}_2 \Psi_0]_{ji} = -\frac{a}{R} \cos \theta_j \sum_{i'} \bar{\Delta}_{ii'} \Phi_{j'i'} \quad (84)$$

$$[\hat{\mathcal{L}}_3 \Psi_0]_{ji} = \frac{a \sin \theta_j}{R \tilde{r}_i} \sum_{j'} \Delta_{jj'} \Phi_{j'i} \quad (85)$$

Hence, finding $\Psi_{0(\text{new})}$ by solving eqn (80) is equivalent to obtaining

$$\Phi_{ji(\text{new})} = \sum_{j'} H_{i,jj'}^{-1} \left[\Phi_{j'i(\text{old})} + \varepsilon \frac{a}{R} \cos \theta_j \sum_{i'} \bar{\Delta}_{ii'} \Phi_{j'i'(\text{old})} \right] \quad (86)$$

where for every given i , $H_{i,jj'}^{-1}$ is the matrix element of the inverse matrix of the $M \times M$ matrix defined by the element

$$H_{i,jj'} \equiv \delta_{jj'} - \varepsilon \left[\Delta_{jj'}^2 + \frac{\cos \theta_j}{\sin \theta_j} \Delta_{jj'} + \frac{a \sin \theta_j}{R \tilde{r}_i} \Delta_{jj'} \right] \quad (87)$$

where $j, j' = 1, 2, 3, \dots, M$.

We pay special attention to properly handle the boundary conditions. While the elements of the H matrix are written in the last paragraph in a general form, the expression must be revised for special cases. At $\theta = 0$, the boundary condition in eqn (55) implies

$$\hat{\mathcal{D}}_1 \Psi_0 = \left(\frac{\partial^2 \Psi_0}{\partial^2 \theta} + \frac{\cos \theta}{\sin \theta} \frac{\partial \Psi_0}{\partial \theta} \right) \bigg|_{\theta=0} = 2 \frac{\partial^2 \Psi_0}{\partial^2 \theta} \bigg|_{\theta=0}. \quad (88)$$

Hence

$$H_{i,1j'} \equiv \delta_{1j'} - 2\varepsilon \Delta_{1j'}^2. \quad (89)$$

Similar modification should be made to $H_{i,Mj'}$.

The hard-wall boundary condition in eqn (56) for $\tilde{r} = 1$ (or $i = N$) can be enforced in an implicit way. At $\tilde{r} = 1$, we require $\Psi_{j,N(\text{new})} = 0$ if $j \geq (M+1)/2$; thus only half of Φ_{jN} ($j \leq (M-1)/2$) need to be calculated from eqn (86),⁶¹ i.e., eqn (86) becomes

$$\Phi_{jN(\text{new})} = \sum_{j'} H_{N,jj'}^{-1} \left[\Phi_{j'N(\text{old})} + \varepsilon \frac{a}{R} \cos \theta_{j'} \sum_{i'} \bar{\Delta}_{Ni'} \Phi_{j'i'(\text{old})} \right] \quad (90)$$

where $H_{N,jj'}$ is a $[(M-1)/2] \times [(M-1)/2]$ matrix which has the same definition in eqn (87) but $j, j' = 1, 2, 3, \dots, (M-1)/2$.

At $\tilde{r} = 0$ ($i = 1$), according to the boundary condition in eqn (53) and (54), we require $\sum_{j'} \Delta_{jj'} \Phi_{j'1} = 0$, $\sum_{j'} \Delta_{jj'}^2 \Phi_{j'1} = 0$ and

$\sum_{i'} \bar{\Delta}_{ii'} \Psi_0 = 0$. Thus $\Phi_{j1(\text{new})}$ should be determined by solving

$$\sum_{i'} \bar{\Delta}_{ii'} \Phi_{ji'(\text{new})} = 0 \quad (91)$$

after all $\Phi_{ji(\text{new})}$ for $i \geq 2$ are obtained. Furthermore, $\Psi_0(\tilde{r}, \theta)$ is actually a constant at $\tilde{r} = 0$. Therefore an additional average was performed to enforce this constraint

$$\Phi_{j1(\text{new})} \leftarrow \frac{\sum_j \sin \theta_j w_j \Phi_{j1(\text{new})}}{\sum_j \sin \theta_j w_j} \quad (92)$$

where w_j is the weight of the j -th Chebyshev node.

Two parameters are defined,

$$\mu_1 = - \frac{\int_0^\pi \int_0^1 [(\Psi_{0(\text{new})} - \Psi_{0(\text{old})})/\varepsilon] \tilde{r}^2 \sin \theta d\tilde{r} d\theta}{\int_0^\pi \int_0^1 \Psi_{0(\text{old})} \tilde{r}^2 \sin \theta d\tilde{r} d\theta}, \quad (93)$$

$$\mu_2^2 = - \frac{\int_0^\pi \int_0^1 [(\Psi_{0(\text{new})} - \Psi_{0(\text{old})})/\varepsilon]^2 \tilde{r}^2 \sin \theta d\tilde{r} d\theta}{\int_0^\pi \int_0^1 (\Psi_{0(\text{old})})^2 \tilde{r}^2 \sin \theta d\tilde{r} d\theta}. \quad (94)$$

The iteration was considered convergent once $|\mu_1 - \mu_2|/\mu_2 \leq 10^{-5}$ and then μ_1 is the numerical solution for μ in eqn (51).

Normalization was made after every update,

$$\Psi_{0(\text{new})} \leftarrow \frac{\Psi_{0(\text{new})}}{\int_0^\pi \int_0^1 \Psi_{0(\text{new})}(\tilde{r}, \theta) \Psi_{0(\text{new})}(\tilde{r}, \pi - \theta) \tilde{r}^2 \sin \theta d\tilde{r} d\theta}, \quad (95)$$

to stabilize the overall numerical scheme. This normalization does not affect the eigen problem in eqn (51), and is used to avoid exponential diminishing of the stored eigenfunction. The

normalized function $\Psi_{0(\text{new})}$, is then used as $\Psi_{0(\text{old})}$ in the next step of iteration.

Larger N and M permit a higher numerical resolution and allow us to describe sharper density distribution $\Psi_0(\tilde{r}, \theta)$ when a/R is small. A finer grid system also requires smaller ε , which is a numerical parameter used to control the convergence of the algorithm. In current work, N , M and ε were set as 80, 401, and 10^{-5} , respectively.

Acknowledgements

The authors acknowledge the financial support from the Natural Science and Engineering Council of Canada, the National Basic Research Program of China (Grant no. 2011CB605700) and the NSF of China (Grant nos 91127033 and 21374023). JZYC thanks Fudan University for a special senior visiting scholarship that enabled this work.

References

- O. Kratky and G. Porod, *Recl. Trav. Chim. Pays-Bas*, 1949, **68**, 1106–1122.
- N. Saitō, K. Takahashi and Y. Yunoki, *J. Phys. Soc. Jpn.*, 1967, **22**, 219–226.
- M. Doi and S. F. Edwards, *The Theory of Polymer Dynamics*, Oxford University Press, New York, 1988.
- T. Odijk, *Macromolecules*, 1983, **16**, 1340–1344.
- M. Dijkstra, D. Frenkel and H. N. Lekkerkerker, *Phys. A*, 1993, **193**, 374–393.
- T. W. Burkhardt, *J. Phys. A: Math. Gen.*, 1997, **30**, L167–L172.
- D. J. Bicout and T. W. Burkhardt, *J. Phys. A: Math. Gen.*, 2001, **34**, 5745–5750.
- Y.-L. Chen, H. Ma, M. D. Graham and J. J. de Pablo, *Macromolecules*, 2007, **40**, 5978–5984.
- P.-K. Lin, C.-C. Fu, Y.-L. Chen, Y.-R. Chen, P.-K. Wei, C. H. Kuan and W. S. Fann, *Phys. Rev. E: Stat., Nonlinear, Soft Matter Phys.*, 2007, **76**, 011806.
- Y. Yang, T. W. Burkhardt and G. Gompper, *Phys. Rev. E: Stat., Nonlinear, Soft Matter Phys.*, 2007, **76**, 011804.
- J. Z. Y. Chen, D. E. Sullivan and X. Yuan, *Macromolecules*, 2007, **40**, 1187–1195.
- T. Cui, J. Ding and J. Z. Y. Chen, *Phys. Rev. E: Stat., Nonlinear, Soft Matter Phys.*, 2008, **78**, 061802.
- T. Odijk, *Phys. Rev. E: Stat., Nonlinear, Soft Matter Phys.*, 2008, **77**, 060901.
- P.-K. Lin, K.-H. Lin, C.-C. Fu, K.-C. Lee, P.-K. Wei, W.-W. Pai, P.-H. Tsao, Y.-L. Chen and W. S. Fann, *Macromolecules*, 2009, **42**, 1770–1774.
- Y. Wang, D. R. Tree and K. D. Dorfman, *Macromolecules*, 2011, **44**, 6594–6604.
- P.-K. Lin, C.-C. Hsieh, Y.-L. Chen and C.-F. Chou, *Macromolecules*, 2012, **45**, 2920–2927.
- Z. Benková and P. Cifra, *Macromolecules*, 2012, **45**, 2597–2608.
- D. R. Tree, Y. Wang and K. D. Dorfman, *Phys. Rev. Lett.*, 2012, **108**, 228105.

- 19 L. Dai, D. R. Tree, J. R. C. van der Maarel, K. D. Dorfman and P. S. Doyle, *Phys. Rev. Lett.*, 2013, **110**, 168105.
- 20 D. R. Tree, Y. Wang and K. D. Dorfman, *Phys. Rev. Lett.*, 2013, **110**, 208103.
- 21 J. Z. Y. Chen, *Macromolecules*, 2013, **46**, 9837–9844.
- 22 H.-P. Hsu and K. Binder, *Soft Matter*, 2013, **9**, 10512.
- 23 H.-P. Hsu and K. Binder, *Macromolecules*, 2013, **46**, 8017–8025.
- 24 Y.-L. Chen, Y.-H. Lin, J.-F. Chang and P.-K. Lin, *Macromolecules*, 2014, **47**, 1199–1205.
- 25 A. Muralidhar, D. R. Tree, Y. Wang and K. D. Dorfman, *J. Chem. Phys.*, 2014, **140**, 084905.
- 26 G. Morrison and D. Thirumalai, *Phys. Rev. E: Stat., Nonlinear, Soft Matter Phys.*, 2009, **79**, 011924.
- 27 D. Reith and P. Virnau, *Comput. Phys. Commun.*, 2011, **182**, 1945–1948.
- 28 M. R. Smyda and S. C. Harvey, *J. Phys. Chem. B*, 2012, **116**, 10928–10934.
- 29 P. Cifra and T. Bleha, *Macromol. Theory Simul.*, 2012, **21**, 15–23.
- 30 T. Odijk, *Macromolecules*, 1993, **26**, 6897–6902.
- 31 P. G. de Gennes, *Scaling Concepts in Polymer Physics*, Cornell University Press, Ithaca, 1979.
- 32 J. Z. Y. Chen, D. E. Sullivan and X. Yuan, *Europhys. Lett.*, 2005, **72**, 89.
- 33 A. Y. Grosberg, A. R. Khokhlov and Y. A. Atanov, *Statistical Physics of Macromolecules*, AIP, New York, 1994.
- 34 K. F. Freed, *Adv. Chem. Phys.*, 1972, **22**, 1–128.
- 35 M. G. Bawendi and K. F. Freed, *J. Chem. Phys.*, 1985, **83**, 2491.
- 36 C. M. Marques and G. H. Fredrickson, *J. Phys. II*, 1997, **7**, 1805–1816.
- 37 K. Ghosh and M. Muthukumar, *J. Polym. Sci., Part B: Polym. Phys.*, 2001, **39**, 2644–2652.
- 38 M. Abramowitz and I. Stegun, *Handbook of Mathematical Functions*, Dover Publishing Inc., New York, 1970.
- 39 Z. Y. Chen, *Phys. Rev. Lett.*, 1993, **71**, 93–96.
- 40 Z. Y. Chen, *Macromolecules*, 1993, **26**, 3419–3423.
- 41 Q. Liang, J. Li, P. Zhang and J. Z. Y. Chen, *J. Chem. Phys.*, 2013, **138**, 244910.
- 42 Y. Jiang and J. Z. Y. Chen, *Phys. Rev. E: Stat., Nonlinear, Soft Matter Phys.*, 2013, **88**, 042603.
- 43 G. B. Arfken, H. J. Weber and L. Ruby, *Mathematical Methods for Physicists*, Academic Press, New York, 1985.
- 44 Z. Y. Chen and S.-M. Cui, *Phys. Rev. E: Stat. Phys., Plasmas, Fluids, Relat. Interdiscip. Top.*, 1995, **52**, 3876–3880.
- 45 J. Z. Y. Chen, *Soft Matter*, 2013, **9**, 10921.
- 46 M. M. A. E. Claessens, R. Tharmann, K. Kroy and A. R. Bausch, *Nat. Phys.*, 2006, **2**, 186–189.
- 47 M. M. A. E. Claessens, M. Bathe, E. Frey and A. R. Bausch, *Nat. Mater.*, 2006, **5**, 748–753.
- 48 A. J. Spakowitz and Z.-G. Wang, *Phys. Rev. Lett.*, 2003, **91**, 166102.
- 49 C.-H. Lin, Y.-C. Tsai and C.-K. Hu, *Phys. Rev. E: Stat., Nonlinear, Soft Matter Phys.*, 2007, **75**, 031903.
- 50 A. Khokhlov and A. Semenov, *Phys. A*, 1982, **112**, 605–614.
- 51 T. C. Lubensky and J. Prost, *J. Phys. II*, 1992, **2**, 371–382.
- 52 D. R. Nelson, *Defects and Geometry in Condensed Matter Physics*, Cambridge University Press, Cambridge, 2002.
- 53 M. J. Bowick and L. Giomi, *Adv. Phys.*, 2009, **58**, 449–563.
- 54 A. M. Turner, V. Vitelli and D. R. Nelson, *Rev. Mod. Phys.*, 2010, **82**, 1301–1348.
- 55 D. G. Angelescu, P. Linse, T. T. Nguyen and R. F. Bruinsma, *Eur. Phys. J. E*, 2008, **25**, 323–334.
- 56 W.-Y. Zhang and J. Z. Y. Chen, *Europhys. Lett.*, 2011, **94**, 43001.
- 57 L. Onsager, *Ann. N. Y. Acad. Sci.*, 1949, **51**, 627–659.
- 58 T. Odijk, *Macromolecules*, 1986, **19**, 2313–2329.
- 59 Y. Jiang and J. Z. Y. Chen, *Macromolecules*, 2010, **43**, 10668–10678.
- 60 Y. Jiang and J. Z. Y. Chen, *Phys. Rev. Lett.*, 2013, **110**, 138305.
- 61 L. N. Trefethen, *Spectral Methods in MATLAB*, SIAM, Philadelphia, 2000.
- 62 S.-M. Hur, C. J. García-Cervera and G. H. Fredrickson, *Macromolecules*, 2012, **45**, 2905–2919.